Shahid Chamran University of Ahvaz

Journal of

Applied and Computational Mechanics

Journal of Applied and Computational Mechanics

Investigation of Driving Torques at the Joints of Industrial Robot Arms based on the Topology Optimization Technique

Duong Xuan Bien[ID]

Advanced Technology Center, Le Quy Don Technical University, Vietnam

Abstract. This paper presents an investigation on the driving torques of industrial robot arm joints using the structural optimization method for Upper Arm (UA) link. The optimal criteria mention reducing the mass of UA link. The static and dynamic analysis problems are considered when robot moves in the vertical plane and in space. Results of these problems are used to perform the optimization of UA link structure. Stress and displacement values in static and dynamic analyses of the optimized link with a weight reduction of 39% and over 45% in volume show that it ensures to meet the set optimal criteria. A mathematical model of 6 degrees of freedom (DOF) robot is established to determine the kinematic and dynamic equations. The inverse kinematic and dynamic problems solving the algorithm of the redundant robot is effectively applied to determine the input values with the given motion trajectory of the end-effector point in the workspace with two different trajectories in a plane and space. The analysis results show that there is a change in driving torque values in a direction favorable for the operation of the joints for any trajectory when the mass of robot reduces. This is also verified by a simple 2DOF robot model presented in the Appendix with three different optimization methods. The reported results have essential implications for application of various topology optimization issues in order to positively change the driving torques at joints while well ensuring the functionality of robot arm.

Keywords: Driving torques, industrial robots, topology optimization, inverse dynamics.

1. Introduction

In the near future, a meaningful number of robots will be used widely with continuous operation frequency and long working cycles in smart factories. Therefore, they are subjected to high energy consumption in production. Finding solutions to reduce energy consumption is an urgent matter in order to minimize the costs and enhance the production efficiency. The problem of reducing costs and improving the machining productivity of robots is solved in many directions such as optimization of machining trajectory [1], feed rate [2], technology parameters [3] and reduction of machining time leads to reduced energy consumption during total process [4].

In the overall energy consumption problem, the driving torques at joints accounts for a fairly high percentage because they are directly related to the actuators and their corresponding efficiency. The links weight in particular and the robot motion trajectory in general have a great influence on the consumption of driving torques [5]. Structural designing to reduce the links weight has also been considered recently such as the flexible robot study [6], the optimization techniques application in the structural design [7]. First of all, the trend of reduced mass is always considering for almost objects moving because the lighter, the more energy efficient. With the robot structure, the lighter the components of the robot, the better it is to save construction materials, reduce inertia in motion, reduce the cost of driving energy, and reduce the load-bearing level of the actuators, convenient in moving between working place. Mass reduction becomes especially important for flying devices. According to [8], each pound of weight saved on a commercial airplane will save 14,000 gallons of aviation fuel a year. Manufacturers of cars, airplanes, robots and other devices are still urgently looking for ways to lighten all the parts of their systems to save fuel. Each component is scrutinized for their structure and function. Of course, some structures should not apply the TO when they are reasonable and need ensuring the safety. Basically, structurally optimized parts will often require less resources to create them such as materials, energy to manufacture, manufacturing processes, sometimes space occupied in the working place. Therefore, optimizing structures using TO technique is still essential, especially when combined with new technologies develop strongly such as metal 3D printing (additive machining), techniques modern machining on multi-axis numerical control machines.

In particular, the TO method [9-25] is preferred to reduce the structural weight of the robot but still ensure the load capacity, control the stress and deformation state of the system. The procedure for performing simple SO is described in [9]. The Solid Isotropic Material with Penalization (SIMP) method for isotropic materials is clearly presented in [10], [11]. The Bi-Evolutionary Structural Optimization (BESO) method is mentioned in [12]. The LEVELSET method is shown in [13], [14]. The TOBS algorithm was developed for submerged structures in [15]. The radial basis function (RBF) algorithm combined with the LEVELSET introduced in [16] to improve the efficiency of structural optimization. TO algorithms are applied in many different fields and objects such as in truss structures [17], Vehicle [18], Humanoid robot [19], Quadcopter [20] and industrial robot (IR) arms [21-25]. SIMP method was used in [21] to optimize the Upper Arm (UA) link on 6DOF industrial robot with a weight reduction of 44.4% but it is not clearly yet.

The results of static and dynamic analysis (SA-DA) show that the After-optimization displacement value is not greater and the natural vibrational frequency value is not lower than that of the Pre-optimization. The multi-objective SO problem including stiffness, vibration frequency and IR mass was performed in [22] with the UA link being optimally selected. Static-dynamic analysis and SO were performed on the HYPERWORKS software. The SO results show that the robot mass is reduced by 7.1%, the static deformation is reduced by 22.4%, and the natural vibration frequency is increased by more than 14%. Similarly, the multi-objective SO problem is also considered for the IR in [23] with the SIMP method. ADAMS and SOLIDWORKS software were used to perform the SA-DA and optimization. A mainly link on the IR arm is optimally analyzed in [24] based on Generative Design (GD) module and TO method for additive manufacturing (AM). The mechanical and microstructural properties of the part using AM were analyzed to evaluate the optimal design quality with a 50% reduction in the weight of the part. The SOLIDWORKS software is used to perform the optimization process. The UA link of industrial welding robots is optimally considered in [25] with ADAMS and AQUABUS software. The reduction of the link weight is 17.9%, the low-order natural frequency is increased. Experimental results show that the After-optimized structure still meets the working capacity compared to the original structure. Some preliminary evaluation among structural optimization techniques applied CAE software are presented in [26].

In summary, some preliminary observations can be made as follows

- Firstly, previous publications mainly mentioned optimization methods such as SIMP, BESO, LEVELSET but only focused on 2D models [10-16] or GD method with 3D models [22-25] or how to increase their effectiveness.
- Secondly, the problem of investigating the driving torques of the joints on the industrial robot arm after structural optimization has not been specifically considered.
- Thirdly, the after-optimal 6DOF robot model needs to be considered for motion trajectories in the workspace. These trajectories need to be planned specifically with velocity and acceleration constraints.

The main contribution of this paper is to investigate the driving torque values of the joints (J2 and J3) related to the optimized UA link (link 2) of the 6DOF industrial robot using TO technique. This requires performing many steps and using complicated calculation methods. Accordingly, the static and dynamic models of the robot are considered in order to find the force and moment values for the optimal expected link. The criteria of mass, stress and displacement are proposed to correspond the boundary conditions of the optimization problem. The driving torque values of joints in Pre-TO and After-TO cases are compared through the IK and ID problems of the redundant robot system with different trajectories in a vertical plane and space. Quantitative results of the driving torque will be the basis for developing the application of TO technique to most other components of the robot or to other similar systems. The content of this study is performed according to the steps shown in Fig. 1.
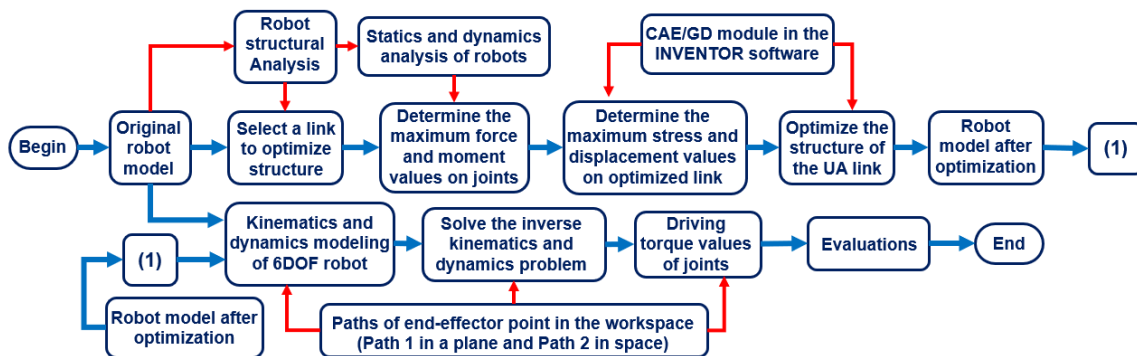

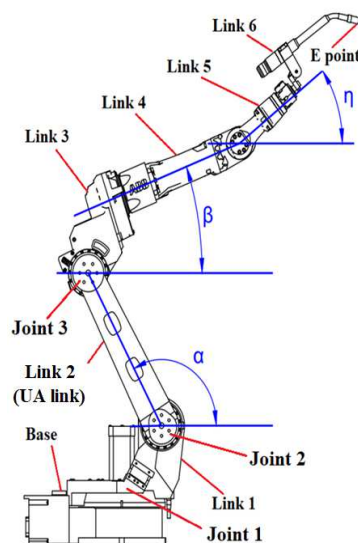**Fig. 1.** Implementation diagram of this research contents.
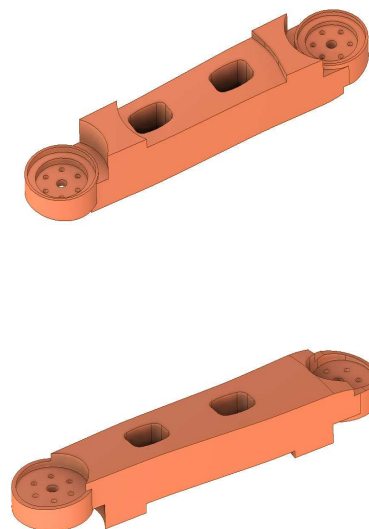

Fig. 2. 6DOF industrial Robot.   **Fig. 3.** The UA link structure in Pre-optimization.
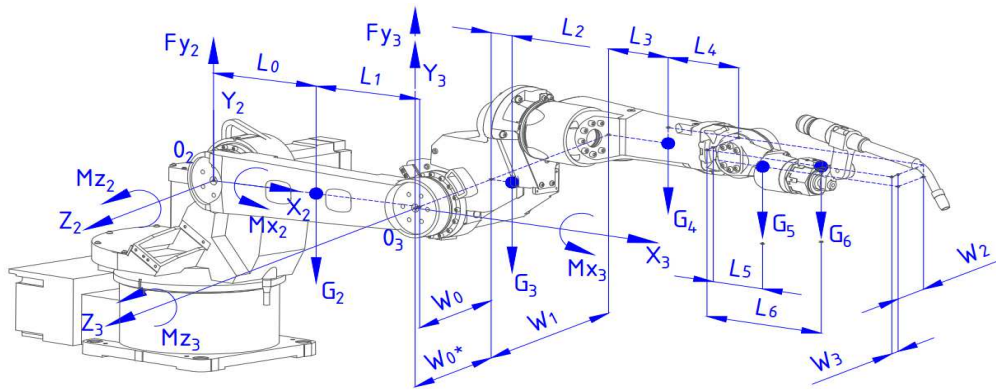
Fig. 4. Calculation position.

2. Materials and Methods

2.1. Static and dynamic analyses for 6DOF robot pre-TO

Industrial robot structure with many degrees of freedom includes different components and all play an important role in performing the working function of robots. Structural optimization of all robot components is impractical. The structure of the robot needs to be analyzed specifically to determine which components should be paid more attention to with specific criteria such as the degree of influence on the ability of the robots to work, the proportion of the mass of the components comparing to the overall mass, the degree of load bearing, the feasibility of applying optimization techniques, etc. The structure of 6DOF industrial welding robot is depicted as shown in Fig. 2. Obviously, joint 1 (J1) is the joint that bears the largest load even when the robot is stationary or motion. Accordingly, the UA link is one of the main moving components and accounts for a significant proportion of the total mass of the robot. Joint 2 (J2) and joint 3 (J3) are respectively subject to heavy load after J1. Considering the role and structure of links on the robot, the UA link is selected for structural optimization (Fig. 3).

It should be noted that before optimization by TO technique it is to simplify the geometry for the UA link. Some of the corners or small grooves are simplified because they are the result of the manufacturing process from the molding, cutting machining or other industrial processing methods. These structures hardly affect the Pre- and After-optimum analysis results. On the other hand, keeping these structures the same will significantly increase the time of finite element meshing and other complex calculations. The process of structural simplification and optimization analysis was performed using INVENTOR software [22]. Due to the copyright nature of industrial products, detailed drawings and important parameters of the UA link fabrication materials are not disclosed. Figure 4 depicts the structure of the UA link after being simplified. J2 and J3 on the UA link are hinge joints.

Considering the problem of static analysis, with each different α, β and η angle values, the force and moment values acting on the joints are also different. Accordingly, the force and torque balance equations at J2 and J3 are determined as follows:

$$\sum F_{xi} = 0; \sum F_{yi} = 0; \sum F_{zi} = 0; \sum M_{xi} = 0; \sum M_{yi} = 0; \sum M_{zi} = 0; \quad (i = 2,3) \tag{1}$$

where F_{xi}, F_{yi}, F_{zi} and $M_{xi}, M_{yi}, M_{zi}; (i = 2,3)$ are the forces and moments acting on J2 and J3 in the coordinate systems $(OXYZ)_2$ and $(OXYZ)_3$, respectively. Forces and moments at J2 are calculated as:

$$\begin{cases} F_{x2} = 0; F_{y2} = G_2 + G_3 + G_4 + G_5 + G_6; F_{z2} = 0; M_{y2} = 0 \\ M_{x2} = G_3 W_0 + G_4 (W_0 + W_1) + G_5 (W_0 + W_1 - W_2) + G_6 (W_0 + W_1 - W_2 - W_3) \\ M_{z2} = G_2 L_0 \cos\alpha + G_3 ((L_0 + L_1)\cos\alpha + L_2\cos\beta) + G_4 (L_0 + L_1)\cos\alpha + G_4 L_3 \cos\beta + G_5 ((L_0 + L_1)\cos\alpha + (L_3 + L_4)\cos\beta + L_5\cos\eta) \\ \quad + G_6 ((L_0 + L_1)\cos\alpha + (L_3 + L_4)\cos\beta + L_6\cos\eta) \end{cases} \tag{2}$$

Forces and moments at J3 are determined as:

$$\begin{cases} F_{x3} = 0; F_{y3} = G_3 + G_4 + G_5 + G_6; F_{z3} = 0 \\ M_{x3} = G_3 W_0^* + G_4 (W_0^* + W_1) + G_5 (W_0^* + W_1 - W_2) + G_6 (W_0^* + W_1 - W_2 - W_3); M_{y3} = 0 \\ M_{z3} = (G_3 L_2 + G_4 L_3)\cos\beta + G_5 ((L_3 + L_4)\cos\beta + L_5\cos\eta) + G_6 ((L_3 + L_4)\cos\beta + L_6\cos\eta) \end{cases} \tag{3}$$

where L_i and $W_i, (i = 0,..,6)$ are the distances between the centers of the joints to the centers of the links in the respective axial directions, respectively. G_2, G_3, G_4, G_5 and G_6 are the weights of the links respectively. Some static positions of the robot are considered corresponding to the values of angles α, β, η as shown in Table 1 to assess the position where joints 2 and 3 bear the maximum loads.

Table 1. Static analysis positions corresponding to angles α, β, η.
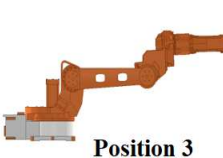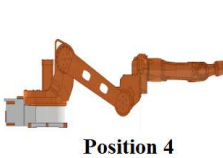

Position 1	Position 2	Position 3	Position 4
$\alpha = 90^o, \beta = \eta = 0^o$	$\alpha = 45^o, \beta = \eta = 0^o$	$\alpha = \beta = \eta = 0^o$	$\alpha = -40^o, \beta = \eta = 0^o$

Table 2. Geometric parameters of the model (Fig. 4) and material properties of the UA link.

Geometric parameters	UA link material	
$L_0 = 0.277; L_1 = 0.313; L_2 = 0.065(mm);$	Parameter	Values
$L_3 = 0.473; L_4 = 0.25; L_5 = 0.08(mm);$	Density (Kg/m³)	7850 kg/m3
$L_6 = 0.272(mm);$	Yield Strength (MPa)	350 MPa
$W_0 = 0.134; W_1 = 0.045; W_2 = 0.03(mm);$	Ultimate Tensile Strength	420 MPa
$W_0^* = 0.154(mm); G_2 = 337(N);$	Young's (elastic) Modulus (Pa)	2×10^5 MPa
$G_3 = 272; G_4 = 207; G_5 = 41; G_6 = 40(N)$	Poisson's Ratio	0.29

Table 3. Force and moment values at J2 and J3.

Pos	Forces (N) and Moments (Nm) at J2						Forces (N) and Moments (Nm) at J3					
	F_{x2}	F_{y2}	F_{z2}	M_{x2}	M_{y2}	M_{z2}	F_{x3}	F_{y3}	F_{z3}	M_{x3}	M_{y3}	M_{z3}
1	0	890	0	84.61	0	188.31	0	560	0	95.8	0	188.31
2	0	890	0	84.61	0	486.58	0	560	0	95.8	0	188.31
3	**0**	**890**	**0**	**84.61**	**0**	**610.12**	**0**	**560**	**0**	**95.8**	**0**	**188.31**
4	0	890	0	84.61	0	511.44	0	560	0	95.8	0	188.31

Without loss of generality, the material of the UA link is assigned as carbon steel in this study. Therefore, its material properties are described in Table 2.

Based on the results of the SA using stress analysis and dynamic simulation modules of the INVENTOR software, the position of the UA link bears the maximum load (when $\alpha = \beta = \eta = 0$ relative to the horizontal plane) and is described as Position 3 (Pos 3) along with its local coordinate system. The results of J2 and J3 static analysis are shown in Table 3. These values are used in analyzing the stress and displacement of the UA link on INVENTOR software.

Considering the dynamic analysis problem, the force and torque values at joints 2 and 3 on UA link can change during robot joints move. The interaction forces from the external environment have small effect on industrial welding robot different other types of robots used in machining such as drilling, milling or pick and place. On the other hand, the velocities of the components in the robot system are usually tiny changed over the entire welding trajectory due to the characteristics of the machining method. This issue is also mentioned in [21, 23]. Due to the complex structure of robot arm with 6DOF. The dynamic analysis problem in this paper is divided into two cases. Case 1 describes the DA of the robot when it moves in a vertical plane (OXZ) from position Pos 3 upwards with the maximum joint velocity 2 is $140(\text{deg}/s)$ in time $t = 0.5(s)$ [27]. The other joints are fixed. Case 2 is considered with the robot moving in space. All joints move at speeds consistent with reality when welding a curve in space. The joints velocities ($\dot{q}_i, i = 1,..,6$) in case 2 are considered to be $\dot{q}_1 = \dot{q}_2 = \dot{q}_3 = 10(\text{deg}/s); \dot{q}_4 = \dot{q}_5 = \dot{q}_6 = 5(\text{deg}/s)$ in time $t = 10(s)$. Fig. 5 and Fig. 6 show the stress of the UA link at the start and end of the trajectory in the workspace in both cases.

The analysis results of force and moment at J2 and J3 in 2 cases are described as shown in Fig. 7. Table 4 describes the results of DA for the robot before optimization in two cases.

According to the results of DA in Table 4, the force and moment acting on J2 and J3 are greatest at the starting point of the motion trajectory (1475.93N and 1434.39N). However, the force and moment values decrease to the lowest at the end point of the trajectory in case 1 (1151.33N and 1103.52N). Therefore, the stress and displacement values are greatest at the starting point and the smallest at the end point. In contrast, the force and moment values in case 2 do not have much difference between the starting and ending points of the trajectory. Accordingly, the corresponding maximum stress and displacement values do not have a high difference. Even so, the force and moment values in case 1 (in a plane) are still larger than in case 2 (in space).

2.2. Structural optimization of the UA link

The geometry optimization problem is reduced to the problem of maximizing the stiffness (or minimizing the softness) of the design structure. In other words, it is the problem of finding the material density distribution in the design space to achieve the highest stiffness or the lowest softness of the part but still satisfy initial boundary conditions such as loads, stress, and displacement. The basic optimization theory problems are presented more clearly in the Appendix. This paper focuses on optimal design by Generative Design application on INVENTOR software [22]. The procedure to update design variables is implemented according to theory in [7, 10]. The diagram of optimization steps by TO technique related to density method is shown in Fig. 8.
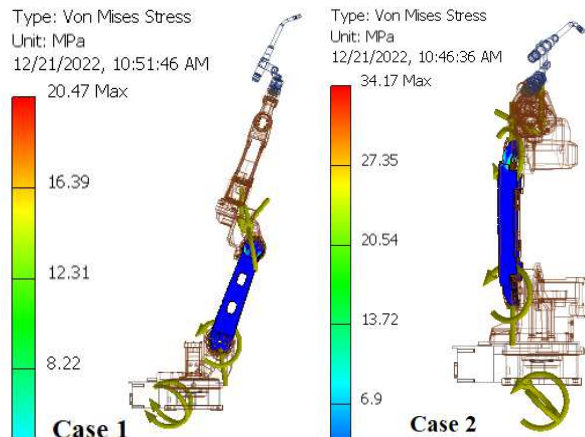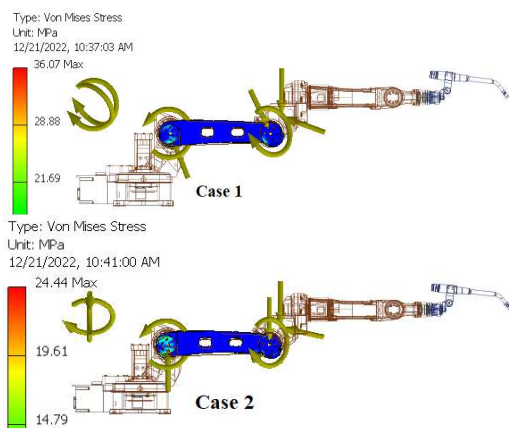

Fig. 5. Stress values of UA link at the starting point in both cases.

Fig. 6. Stress values of UA link at the end point of the trajectory in both cases.

Table 4. Results of DA before optimization.

Joints	Values	Case 1 (in a plane) $(t = 0.5(s))$		Case 2 (in space) $(t = 10(s))$	
		Start position	End position	Start position	End position
Joint 2	$F_{2\,max}(N)$	1475.93	888.66	1434.39	1432.11
	$M_{2\,max}(Nm)$	937.65	218.66	937.28	135.36
Joint 3	$F_{3\,max}(N)$	1151.33	610.69	1103.52	1101.52
	$M_{3\,max}(Nm)$	280.69	84.94	243.72	240.08
S_{max} , D_{max}	$S_{max}(MPa)$	36.07	20.47	24.44	34.17
	$D_{max}(mm)$	0.038	0.026	0.024	0.054
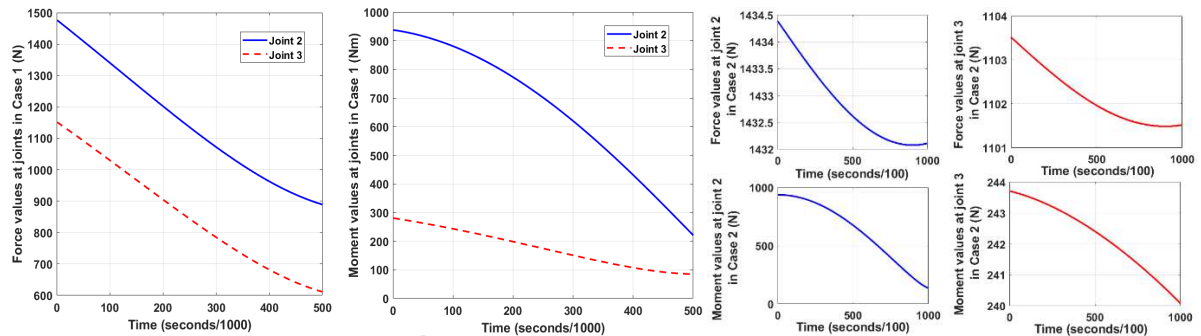
Fig. 7. Force and moment values at J2 and J3 in both cases.
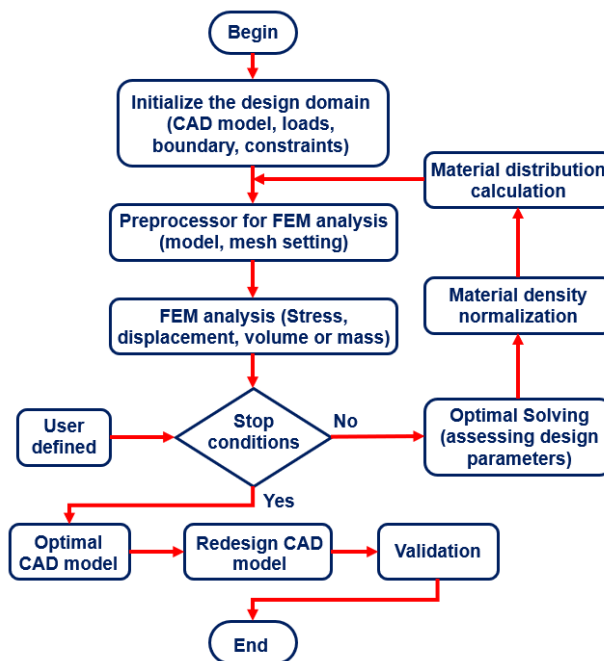
Fig. 8. TO optimization method's scheme.

(a) Stress in Pre-TO   (b) Stress in after-TO   (c) Displacement in after-TO
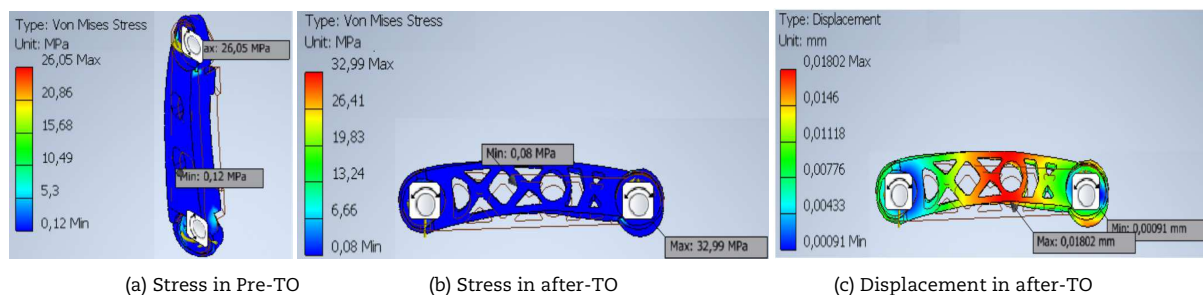
Fig. 9. Static analysis results of Pre-TO and after-TO.

Table 5. After-optimization DA results.

Joints	Values	Case 1 (in a plane) ($t = 0.5(s)$)		Case 2 (in space) ($t = 10(s)$)	
		Start position	End position	Start position	End position
Joint 2	$F_{2\max}(N)$	1349.03	785.02	1306.23	1304.06
	$M_{2\max}(Nm)$	903.14	225.34	902.88	145.29
Joint 3	$F_{3\max}(N)$	1150.74	614.92	1103.52	1101.52
	$M_{3\max}(Nm)$	280.53	85.48	243.72	240.59
$S_{\max}$, $D_{\max}$	$S_{\max}(MPa)$	39.13	19.18	26.33	35.86
	$D_{\max}(mm)$	0.074	0.046	0.048	0.092

Table 6. Comparison of force and torque values of pre-TO and after-TO in DA.

Joints	Values	Case 1 (in a plane) ($t = 0.5(s)$)			Case 2 (in space) ($t = 10(s)$)		
		Start position			Start position		
		Pre-TO	After-TO	Deviation	Pre-TO	After-TO	Deviation
Joint 2	$F_{2\max}(N)$	1475.93	1349.03	126.9	1434.39	1306.23	128.16
	$M_{2\max}(Nm)$	937.65	903.14	34.51	937.28	902.88	34.4
Joint 3	$F_{3\max}(N)$	1151.33	1150.74	0.59	1103.52	1103.52	0
	$M_{3\max}(Nm)$	280.69	280.53	0.16	243.72	243.72	0
$S_{\max}$, $D_{\max}$	$S_{\max}(MPa)$	36.07	39.13	3.06	24.44	26.57	2.13
	$D_{\max}(mm)$	0.038	0.074	0.036	0.024	0.048	0.024

Based on the actual requirements of the structure of UA link, some optimal criteria are determined as follows: the volume of UA link is reduced by at least 30%. In SA and DA, the maximum stress value increases not more than 10MPa, the maximum displacement increases not more than 0.1mm compared to before optimization. Figure 9 depicts UA link Pre-TO and after-TO.

Conduct DA for the robot after optimization with cases 1 (the trajectory of the EEP moves in a plane) and case 2 (the trajectory of the EEP moves in space) as presented above. Velocity values are kept as before optimization in both cases. Figure 10 and Fig. 11 depicts the stress values of the UA link at the starting and ending points of the trajectories. The results of the post-optimized dynamic analysis are shown in the Table 5.
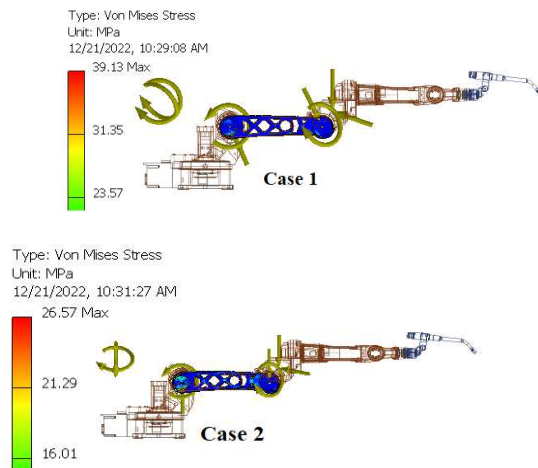

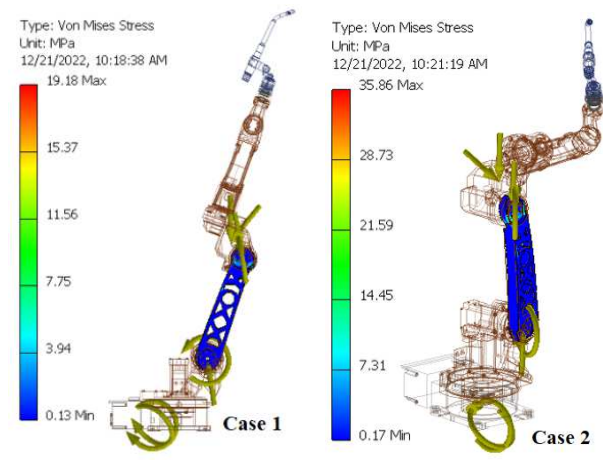**Fig. 10.** Stress values of UA link at the start position in both cases.

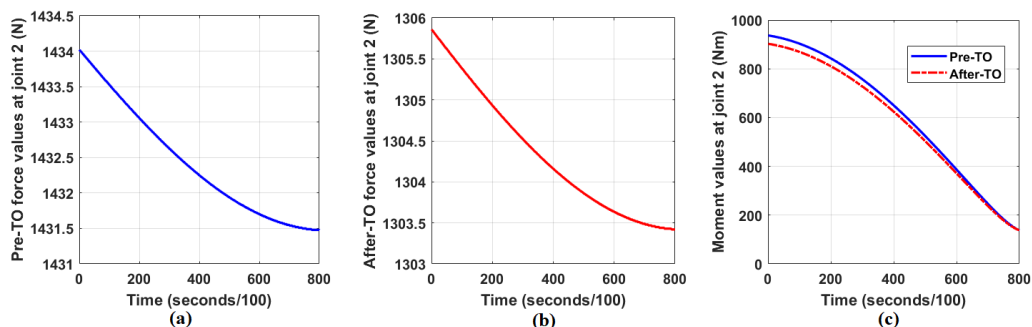**Fig. 11.** Stress values of UA link at the end position in both cases.
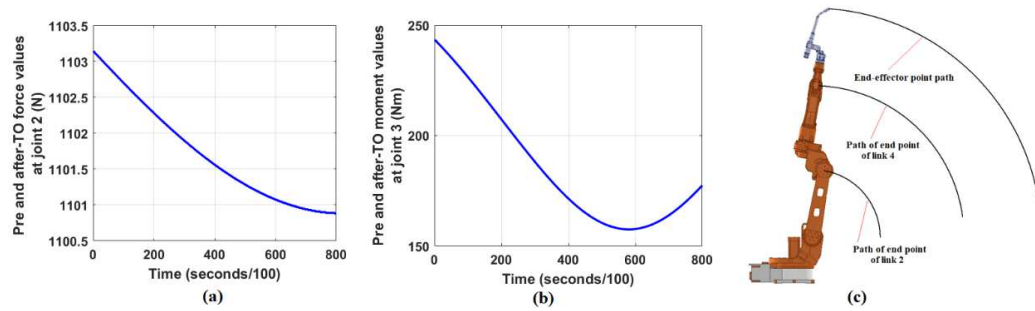

Fig. 12. Force and moment values at J2 in Case 1.

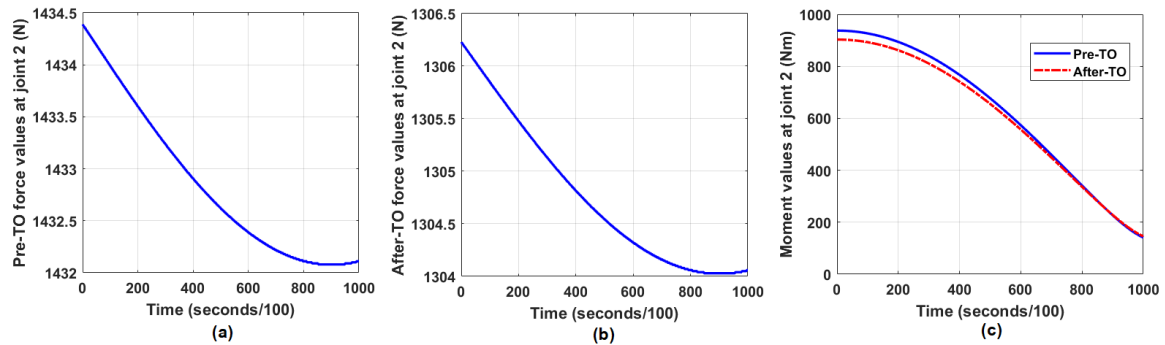**Fig. 13.** Force and moment values at J3 in Case 1.

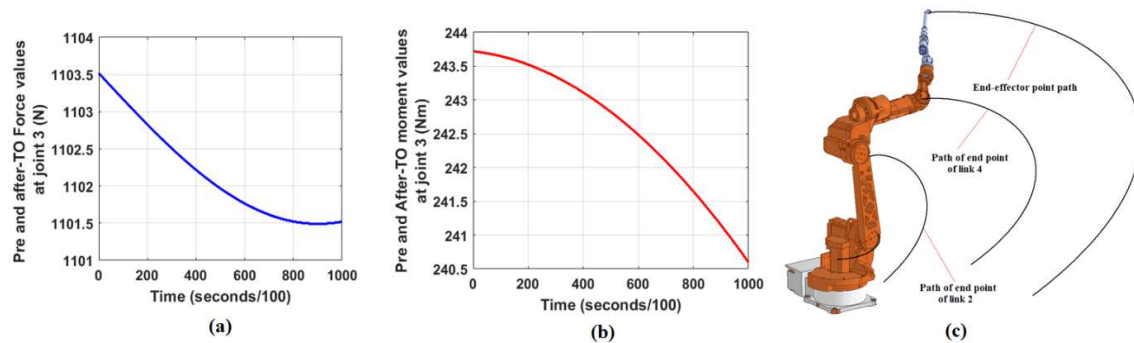**Fig. 14.** Force and moment values at J2 in Case 2.

Fig. 15. Force and moment values at J3 in Case 2.

Table 7. Parameters comparison before and after optimization of UA link structure.

Criteria	Pre-TO	After TO	Unit	Deviation	Goals	Evaluate
Volume	4.3×10^{-3}	2.36×10^{-3}	m^3	Decrease 45.12%	30%	Done
Mass	33,73	20,66	Kg	Decrease 38.75%	30%	Done
Static Analysis						
Criteria	Pre-TO	After TO	Unit	Deviation	Goals	Evaluate
Max. Stress	26.05	32.99	MPa	Increase 6.95 MPa	≤10MPa	Done
Max. Displacement	0.0119	0.0180	mm	Increase 0.0061 mm	≤0.1mm	Done
Dynamic Analysis						
Criteria	Pre-TO	After TO	Unit	Deviation	Goals	Evaluate
Case 1 (trajectory of the EEP in a plane)						
Max. Stress	36.07	39.13	MPa	Increase 3.06 MPa	≤10MPa	Done
Max. Displacement	0.038	0.074	mm	Increase 0.036 mm	≤0.1mm	Done
Case 2 (trajectory of the EEP in space)						
Max. Stress	24.44	26.57	MPa	Increase 2.13 MPa	≤10MPa	Done
Max. Displacement	0.024	0.048	mm	Increase 0.024 mm	≤0.1mm	Done

Table 7 describes the results of the evaluation of the criteria after optimization compared with the initial one.

The actual numerical simulation in static analyzing of different cases shows that, when the mass reduction exceeds 39%, the maximum stress and maximum displacement values exceed the initially set criteria. Therefore, the optimal result of UA link meets the criteria considered for the case with a weight loss of 38.7% or 45.12% in volume. In all the cases including SA and DA or considering the robot's moving trajectory in a plane or in space, the stress and displacement values of the UA link after-TO increase compared to the pre-TO. However, those values are within the allowable range and achieve the initial set goal. The stress value increases the smallest when the robot moves along the trajectory in space. This can be explained by the fact that structures are subjected to forces and moments from many directions. In contrast, when the robot only moves in a vertical plane, the structures are only affected by forces and moments in a certain direction. Their value is larger than when the robot moves with its trajectory in space.

2.3. Kinematic and dynamic modeling of 6DOF robot arm

The kinematic model is presented with DH parameters described in Fig. 16.

Based on the homogeneous transformation matrices [28], the kinematic equations $\mathbf{x}_{EEP} = f(\mathbf{q})$ is established. Where, $\mathbf{X}_{EEP} = [x_E \quad y_E \quad z_E]^T$ is the coordinate vector of the EEP following fixed coordinate system $(OXYZ)_0$ and $\mathbf{q} = [q_1 \quad q_2 \quad q_3 \quad q_4 \quad q_5 \quad q_6]^T$ is the generalized vector of robot. The dynamic equations show the relationship between forces and torques with the motion characteristics of robots such as joint position $\mathbf{q}$, velocity $\dot{\mathbf{q}}$, joint acceleration $\ddot{\mathbf{q}}$. The dynamic equations of the robot are described as follows [29]:

$$\mathbf{M}(\mathbf{q})\ddot{\mathbf{q}} + \mathbf{C}(\mathbf{q}, \dot{\mathbf{q}})\dot{\mathbf{q}} + \mathbf{g}(\mathbf{q}) = \boldsymbol{\tau} \tag{4}$$

where, $\mathbf{M}(\mathbf{q})$ is the mass matrix, $\mathbf{C}(\mathbf{q}, \dot{\mathbf{q}})$ is Coriolis matrix, $\mathbf{g}(\mathbf{q})$ is the gravity vector, $\boldsymbol{\tau} = [\tau_1 \quad \tau_2 \quad .. \quad \tau_6]^T$ is the joints driving torque vector. The components of Eq. (11) are determined similarly in [29]. The generalized vectors $\mathbf{q}, \dot{\mathbf{q}}, \ddot{\mathbf{q}}$ and $\ddot{\mathbf{q}}$ are calculated from solving the IK problem through equation $\mathbf{q} = f^{-1}(\mathbf{x}_E)$. Consider the torch trajectory in the workspace in two cases as follows:

Path 1: $x_E = 0.5 + 0.3(0.1 + \sin\frac{3t}{2}\cos\frac{t}{2})(m)$; $y_E = 0.5 + 0.3(0.1 + \sin\frac{3t}{2}\sin\frac{t}{2})(m)$; $z_E = 0.4(m)$,

and Path 2: $x_E = 1.075 + 0.3\sin\frac{3t}{4}(m)$; $y_E = 0$; $z_E = 1.11 + 0.3\cos\frac{3t}{4}(m)$.

2.4. Assessment the driving torques of joints

This section describes solving the ID problem in the workspace. Firstly, the IK problem is solved based on the AGV method [29, 31] applied to the redundant system with the Path 1 and Path 2 trajectories of the given EEP point. Accordingly, the position, velocity and acceleration of the joints are determined. These values are input to calculate the torque values of the joints through the ID problem. Figure 17 shows the implementation diagram of the inverse dynamics problem using MATLAB/SIMULINK software.
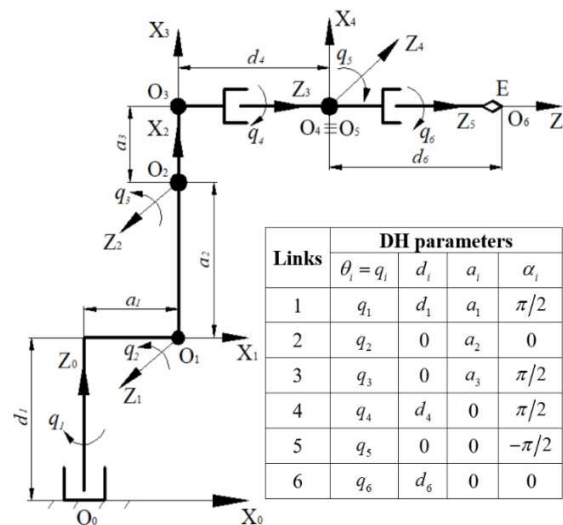

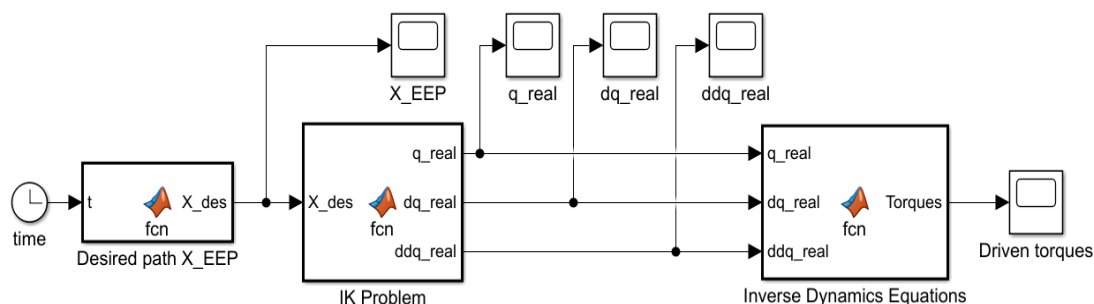**Fig. 16.** Kinematic model of the 6DOF robot and DH parameters.

Links	DH parameters			
	$\theta_i = q_i$	d_i	a_i	α_i
1	q_1	d_1	a_1	$\pi/2$
2	q_2	0	a_2	0
3	q_3	0	a_3	$\pi/2$
4	q_4	d_4	0	$\pi/2$
5	q_5	0	0	$-\pi/2$
6	q_6	d_6	0	0

Fig. 17. The calculation diagram for the inverse dynamic problem in MATLAB/SIMULINK.

Table 8. Dynamics parameters.

Links	J1	J2 - TO		J3	J4	J5	J6
		Before	After				
Mass (kg)	140.32	33.73	20.66	27.2	20.7	4.15	4.0
Gravity center in OX (10^{-3} m)	57.14	160	188.06	78.27	0.061	0.086	-1.0
Gravity center in OY (10^{-3} m)	0.61	730.08	190.45	65.48	-58.1	80.04	-43.0
Gravity center in OZ (10^{-3} m)	-141.06	131.56	674.42	12.79	-249.67	37.66	-34.3
Inertial moment in OX (kg.m^2)	2.485	1.003	0.75	0.839	0.891	0.024	0.034
Inertial moment in OY (kg.m^2)	3.326	0.065	0.04	0.972	0.86	0.005	0.026
Inertial moment in OZ (kg.m^2)	2.722	1.038	0.78	1.046	0.082	0.024	0.01

Geometric parameters of the robot include $d_1 = 0.45(m)$, $a_1 = 0.15(m)$, $a_2 = 0.4(m)$, $a_3 = 0.08(m)$, $d_4 = 0.53(m)$, and $d_6 = 0.097(m)$. Dynamics parameters of the system pre-TO and after-TO are shown in Table 8.

The IK problem for the 6DOF robot is solved based on the AGV method [29]. Calculation results of joint position values for different trajectories are shown in Fig. 18 and Fig. 19.

These results are used to replot the corresponding trajectories that are shown in Fig. 20 and Fig. 21. The numerical simulation results show the reliability of the calculations.

The ID problem results solution of the 6DOF robot pre-TO and after-TO show that the driving torque of joints 3, 4, 5 and joint 6 does not change. Only the torque value of J1 and J2 changes. These values are described from Fig. 22 to Fig. 25.

Torque values of J1 and J2 corresponding to trajectory in Path 1 are shown in Fig. 22 and Fig. 24. Accordingly, the value of torque deviation for J1 is shown (Fig. 22) pre-TO and after-TO are not much different. The maximum deviation value is 4(Nm).

The deviation value of J2 (Fig. 24) pre-TO and after-TO is larger than that of J1. This value is about 100 (Nm). However, it should be noted that the maximum driving torque value before and after the optimum is about 490 (Nm). This shows that, whether optimal or not, the drive motor power selected to drive J2 remains unchanged. Reducing the load of J2 during the movement on the same trajectory is the advantage when optimizing UA link. Similarly, the driving torques of J1 and J2 corresponding to trajectory in Path 2 are shown in Fig. 23 and Fig. 25. Accordingly, the value of torque deviation of J1 is tiny (less than 1 (Nm)), the maximum torque deviation value of J2 is over 100 (Nm). Torque intensity at most trajectory positions in the work space is reduced. On the other hand, the slope produced by the variation of the torque values also decreases after optimization. This leads to an increase in joint endurance. As a result, the life of the joints and the transmission motor is enhanced. Obviously, the reduction in the volume of UA link reaching 39% compared to the original certainly has an effect on the whole system. First for UA link, the changed parameters include mass value, center of gravity position and moment of inertia values. However, a quantitative investigation of the driving torques of these joints is essential to assess the load level of the joints and their life.
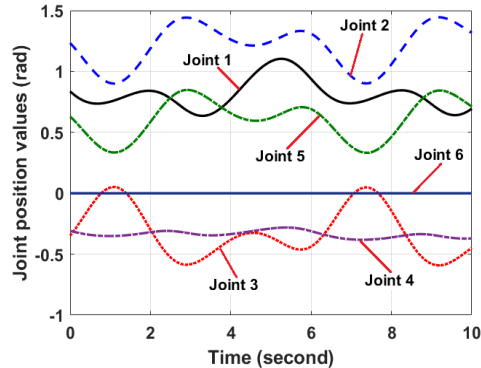

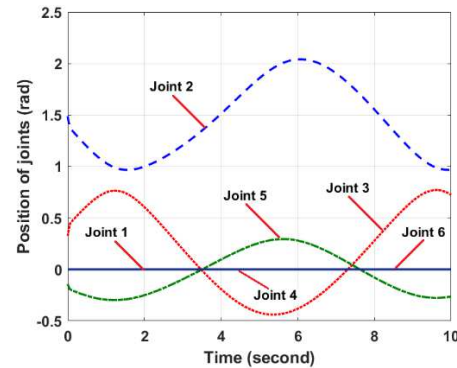**Fig. 18.** Position joints in Path 1.
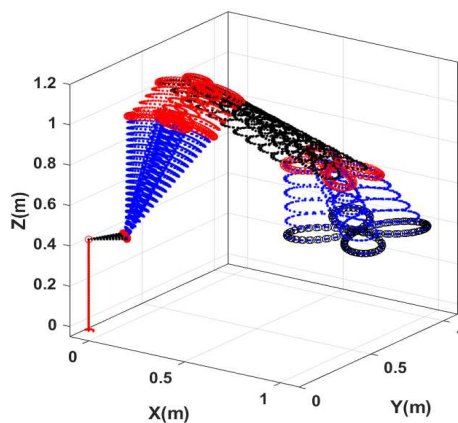

Fig. 19. Position joints in Path 2.

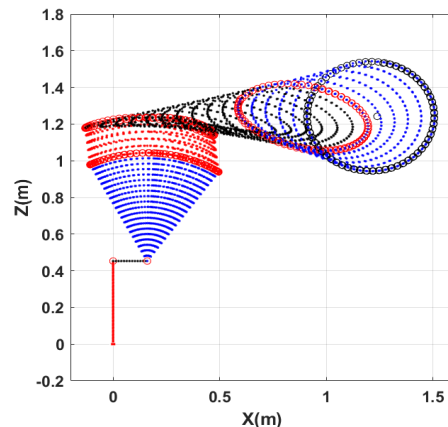**Fig. 20.** The trajectory in Path 1.
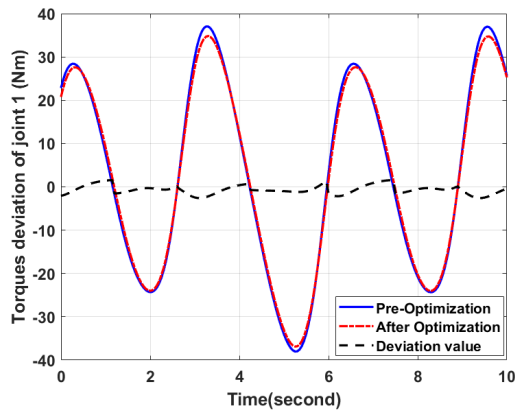

Fig. 21. The trajectory in Path 2.

Fig. 22. J1 torque values - Path 1.
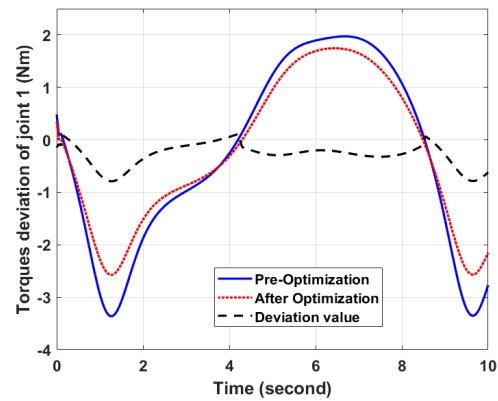

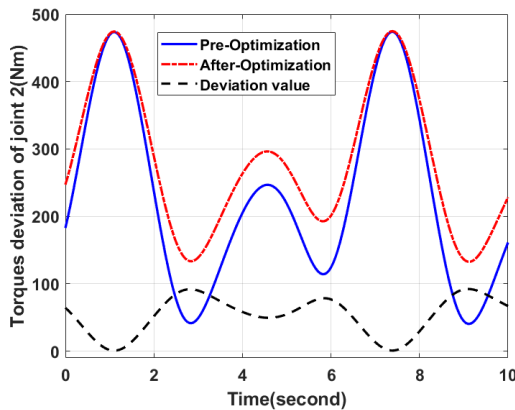**Fig. 23.** J1 torque values - Path 2.
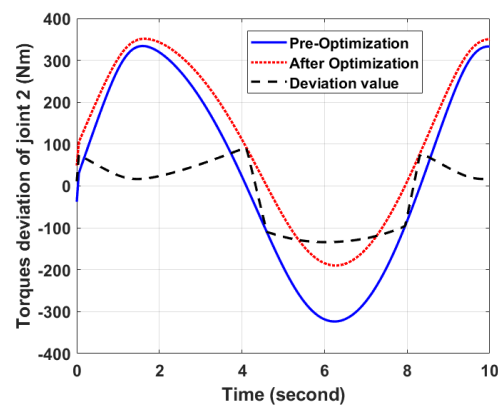

Fig. 24. J2 torque values - Path 1.

Fig. 25. J2 torque values - Path 2.

3. Conclusions

In summary, this paper presented the optimization process of the UA link geometry for 6DOF industrial robot by TO technique and investigated the driving torque at joints through solving the redundant robot ID problem. The loads of J2 and J3 placed on UA link were determined through systematic static and dynamic analyses at the position of the maximum load of the UA link. These values were the inputs to the pre-optimal and after-optimal stress and displacement analysis based on the Generative Design module on the Inventor software. The results of stress and displacement analysis of the optimized part with a weight reduction of 39% and over 45% in volume showed that the optimal structure ensures to meet the set optimal criteria. The kinematic and dynamic equations established for a redundant robot based on DH method allowed to determine the driving torque of joints with 2 different trajectories in the workspace.

Some important points are recognized as follows:

- The numerical results presented that the magnitude and rate of change of the torque value for the optimal structure are smaller than those before the optimal structure. This shows that the load-bearing level of J1 and J2 is lower than Pre-TO leading to increased joint life.
- The SA and DA of the system are necessary to be able to accurately assess the stress and displacement states of the components. Furthermore, the motions of the robot in plane and space both need to be considered. The force and moment values acting on the joints when the robot moves with a trajectory in space do not change much compared to when moving with a trajectory in a plane.
- SIMP and BESO methods showed higher efficiency than GD method when optimizing 2D structures. However, it is not possible to draw similar conclusions with 3D geometric structures. However, the initial GD method shows its intuitiveness and convenience in choosing the optimal solution better than the other methods.
- On the other hand, several geometrical properties of the trajectory in the workspace need to be considered simultaneously while applying the TO techniques.
- Besides, some other criteria such as position accuracy, velocity value, acceleration and jerk of the joints will be mentioned with dynamic loads and system vibration in further studies in the near future.
- Last but not least, the multi-objective topology optimization problem needs to be considered because of the complexity of the overall structure and the ever-changing motion with high speed and high frequency of the robot.

Author Contributions

Not applicable.

Acknowledgments

Conflict of Interest

There are no potential conflicts of interest with respect to the research, authorship, and publication of this article.

Funding

The author received no financial support for the research, authorship, and publication of this article.

Data Availability Statements

The datasets generated and/or analyzed during the current study are available from the corresponding author on reasonable request.

Nomenclature

TO	Topology Optimization	UA	Upper Arm
SO	Structural Optimization	SA	Static Analysis
GD	Generative Design	DA	Dynamic Analysis
DOF	Degrees of Freedom	IR	Industrial Robot
SIMP	Solid Isotropic Material with Penalization	S_{max}	Max. stress value
BESO	Bi-Evolutionary Structural Optimization	D_{max}	Max. displacement value
IK	Inverse Kinematics	J2	Joint 2
ID	Inverse Dynamics	J3	Joint 3
RBF	Radial Basis Function	CAE	Computer-Aided Engineering
AM	Additive Manufacturing	EEP	End-Effector Point

References

[1] Liu, Y., Tian, X., Robot path planning with two-axis positioner for non-ideal sphere-pipe joint welding based on laser scanning, *International Journal of Advanced Manufacturing Technology*, 105(1–4), 2019, 1295–1310.

[2] Liang, L., Zhao, J., Ji, S., An iterative feed rate scheduling method with confined high-order constraints in parametric interpolation, *International Journal of Advanced Manufacturing Technology*, 92(5–8), 2017, 2001-2015.

[3] Sterling, T., Chen, H., Robotic welding parameter optimization based on weld quality evaluation, *6th Annual IEEE International Conference on CYBER Technology in Automation, Control, and Intelligent Systems*, 2016.

[4] Garcia, R.R., Bittencourt, A.C., Villani, E., Relevant factors for the energy consumption of industrial robots, *Journal of the Brazilian Society of Mechanical Sciences and Engineering*, 40(9), 2018, 1–15.

[5] Paryanto, M., Brossog, M., Bornschlegl, M., Franke, J., Reducing the energy consumption of industrial robots in manufacturing systems, *International Journal of Advanced Manufacturing Technology*, 78(5–8), 2015, 1315-1328.

[6] My, C.A., Bien, D.X., Le, C.H., Packianather, M., An efficient finite element formulation of dynamics for a flexible robot with different type of joints, *Mechanism and Machine Theory*, 134, 2019, 267-288.

[7] Bendsoe, M., Kikuchi, N., Generating Optimal Topologies in Structural Design Using a Homogenization Method, *Computer Methods in Applied Mechanics and Engineering*, 71, 1988, 197-224.

[8] https://www.nbcnews.com/id/wbna25592648 (Accessed in Dec 20, 2022).

[9] Xie, Y.M., Steven, G.P., A Simple Evolutionary Procedure for Structural Optimization, *Computer & Structures*, 49(5), 1993, 885-896.

[10] Bendsoe, M.P., Sigmund, O., *Topology Optimization - Theory, Methods and Applications*, Springer-Verlag, New York, 2004.

[11] Erik, A., Anders, C.C., Mattias, S., Boyan, S.L., Sigmund, O., Efficient topology optimization in MATLAB using 88 lines of code, *Structural and Multidisciplinary Optimization*, 43, 2011, 1–16.

[12] Simonetti, H.L., Almeida, V.S., Neves, F.A., Almeida, V.D.D., Topology Optimization for Elastic Analysis of 3D Structures using Evolutionary Methods, *Proceedings of the XLIbero-LatinAmerican Congress on Computational Methods in Engineering*, Brazil, November 11-14, 2019.

[13] Wang, M.Y., Wang, X., Guo, D., A level set method for structural topology optimization, *Computer Methods in Applied Mechanics and Engineering*, 192, 2003, 227–246.

[14] Wei, P., Li, Z., Li, X., Wang, M.Y., An 88-line MATLAB code for the parameterized level set method based topology optimization using radial basis functions, *Structural and Multidisciplinary Optimization*, 58, 2018, 831–849.

[15] Mendes, E., Sivapuram, R., Rodriguez, R., Sampaio, M., Picelli, R., Topology optimization for stability problems of submerged structures using the TOBS method, *Computers and Structures*, 259, 2022, 106685.

[16] Wang, S., Wang, M.Y., Radial basis functions and level set method for structural topology optimization, *International Journal for Numerical Methods in Engineering*, 65, 2005, 2060–2090.

[17] Yan, S., Bai, Y., Zhou, Y., Reduction of truss topology optimization, *Journal of Shanghai University (English Edition)*, 13, 2009, 489–496.

[18] Nilsson, P., *Topology Optimization of a Swing Arm for a Track Driven Vehicle*, Thesis at the Department of Physics, Umea University, Sweden, 2018.

[19] Albers, A., Ottnad, J., System Based Topology Optimization as Development Tools for Lightweight Components in Humanoid Robots, *8th IEEE-RAS International Conference on Humanoid Robots*, Daejeon, Korea, 2008.

[20] Sagar, N., Esakki, B., Lung-Jieh, Y., Chandrasekhar, U., Vepa, K.S., Design and Development of Unibody Quadcopter Structure Using Optimization and Additive Manufacturing Techniques, *Designs*, 6, 2022, 1-25.

[21] Yunfei, B., Ming, C., Yongyao, L., Structural Topology Optimization for a Robot Upper Arm Based on SIMP Method, *Mechanisms and Machine Science*, 36, 2016, 725-733.

[22] Chu, X., Xu, H., Shao, G., Zheng, W., Multi-objective Topology Optimization for Industrial Robot, *Proceedings of the IEEE International Conference on Information and Automation Ningbo*, China, 2016.

[23] Srinivas, G.L., Javed, A., Multi-body dynamic optimization for upper arm of industrial manipulator, *AIP Conference Proceedings*, 2281, 2020, 020022.

[24] Kumaran, M., Senthilkumar, V., Generative Design and Topology Optimization of Analysis and Repair Work of Industrial Robot Arm Manufactured Using Additive Manufacturing Technology, *IOP Conference Series: Materials Science and Engineering*, 1012, 2021, 012036.

[25] Yao, P., Zhou, K., Lin, Y., Tang, Y., Light-Weight Topological Optimization for Upper Arm of an Industrial Welding Robot, *Metals*, 9, 2019, 1020.

[26] https://www.engineering.com/story/research-report-generative-design-and-topology-optimization-in-depth-look-at-the-two-latest (Accessed in Dec 22, 2022).

[27] https://new.abb.com/products/robotics/industrial-robots/irb-1520id (Accessed in October 10, 2022).

[28] Spong, M.W., Hutchinson, S., Vidyasagar, M., *Robot modeling and Control*, First edition, New York, USA, 2001.

[29] Khang, N.V., *Dynamics of Multi-bodies*, Hanoi Science and Technology Publishing House, 2007.

[30] Reza, N.J., *Theory Applied Robotics - Kinematics, Dynamics, and Control*, Springer, New York, 2010.

[31] Bien, D.X., On the Effect of the End-effector Point Trajectory on the Joint Jerk of the Redundant Manipulators, *Journal of Applied and Computational Mechanics*, 7(3), 2021, 1575-1582.

Appendices

P1. Structure optimization problem

The problem of structural optimization can be described by the following equation as:

$$\min_x : \mathbf{C}(\mathbf{X}) = \mathbf{F}^T\mathbf{U} = \mathbf{U}^T\mathbf{K}\mathbf{U} \tag{5}$$

with $\mathbf{X} = \{x_e\}, x_e \in R; 0 \leq x_e \leq 1; \forall e = 1,..,N$; $\mathbf{F} = \mathbf{K}\mathbf{U}$; $\min : V(\mathbf{X}) = \sum x_e v_e = V^*$. Where $\mathbf{C}(\mathbf{X})$ is the objective function of the optimization problem and it is the softness of the structure. $\mathbf{F}$ and $\mathbf{U}$ are force and displacement vectors, respectively. $\mathbf{K}$ is the global stiffness matrix. $\mathbf{X}$ and x_e are the distribution density vector and the distribution density of the element, respectively (with values from 0 to 1). $V(\mathbf{X})$ and v_e are the total volume of the design space and the volume of the element. Finally, V^* is the expected volume, respectively. Some input parameters need to be established for the optimization problem such as: volume ratio needs to be kept V^* and original volume of design space $V(\mathbf{X})$, density correction factor for internal material distribution design space $p = 2 \div 4$. Filter radius value F_R. This is the maximum distance from one element to another that needs to be removed in the sensitivity filter. According to the general Hooke's law, the softness matrix of an element in a finite element grid interpolated from an empty to dense distribution can be written as:

$$\mathbf{C}_e(x_e) = \mathbf{E}_e(x_e)\mathbf{C}_e^0 \tag{6}$$

where $\mathbf{C}_e^0$ is the elastic modulus of the material. This value depends on the Poisson coefficient (ν) for isotropic materials. $\mathbf{E}_e$ is the Young's elastic modulus of each element and is defined as:

$$\mathbf{E}_e(x_e) = x_e^p E_0; p > 1 \tag{7}$$

Using the finite element method, the element stiffness matrix will be calculated in the volume of that element and written using the following formula as:

$$\mathbf{K}_e(x_e) = \mathbf{E}_e(x_e)\mathbf{K}_e^0 \tag{8}$$

Using the interpolation function, the stiffness matrix of all elements in the finite element grid is determined as follows:

$$\mathbf{K}(x_e) = \sum_{i=1}^{N}[E_{min} + x_e^p(E_0 - E_{min})]\mathbf{K}_e^0 \tag{9}$$

Finally, the displacement of an element node can be determined by the following equilibrium formula as:

$$\mathbf{K}(x_e)\mathbf{U}(x_e) = \mathbf{F} \tag{10}$$

where $\mathbf{F}$ is the force vector at the nodes and it depends on the density of material distribution at that element. Typical optimization design methods such as SIMP [10], BESO [11] and LEVELSET [13] all have different advantages and limitations for each structure and specific optimization goals. The density method sensitivity function is described as:

$$\frac{\partial \mathbf{C}}{\partial x_e} = \frac{\partial(\mathbf{U}^T\mathbf{K}\mathbf{U})}{\partial x_e} \tag{11}$$

The optimal goal is usually determined through the following constraints as Stress constraints is $\sigma_{max} \leq [\sigma_a]$. Where σ_{max} is maximum stress and $[\sigma_a]$ is the allowable stress of the structure. Displacement (or strain) constraints is $\Delta_{max} \leq [\Delta_a]$. Where Δ_{max} is the maximum actual displacement (strain) when subjected to external force and $[\Delta_a]$ is the allowable displacement (strain) of the structure. Volume (mass) constraints: $\min V^*$ with $V^* < V$. In most cases, assuming the material is homogeneous and isotropic, this constraint may correspond to a constraint on the total mass or the cross-section area of the structure depending on the particular conditions.

P2. Brief investigation results of driving torque for 2DOF robot based on SO technique

This appendix section shows the optimization results of 2DOF robot's link structure with three methods including SIMP, BESO and GD. The material of all components of the robot is assumed to be Aluminum 6061. A load of 10N is attached at the EEP of 2DOF robot. Optimal results are obtained based on the implementation of static - dynamic analysis steps and structural optimization methods mentioned above. Fig. P1 shows the optimal results of the second link. The kinematic-dynamic parameters of the two-link planar robot are presented in Table PT1. The mathematical model and the dynamics equations can be considered in [30]. The criteria and results of the Pre-TO and after-TO analysis are described in Table PT2
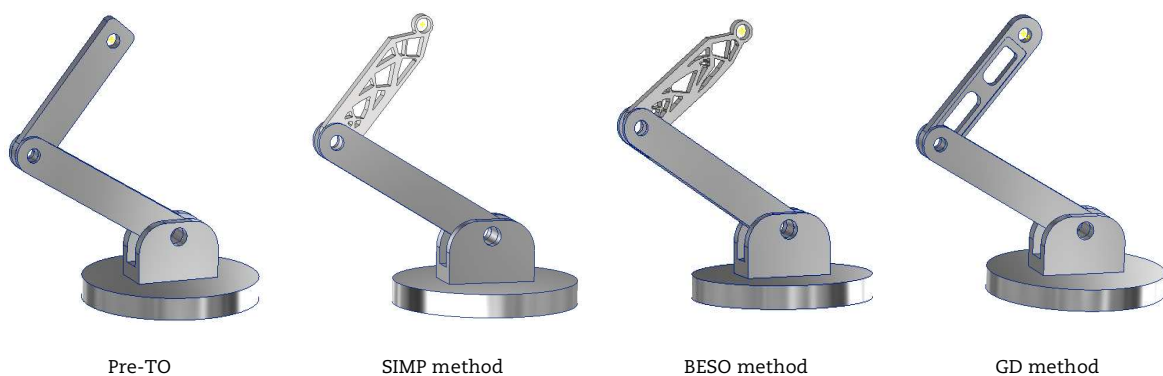

| Pre-TO | SIMP method | BESO method | GD method |

Fig. P1. 2DOF robot model in pre-TO and after-TO.

Table PT1. Kinematics and dynamics parameters of 2DOF planar robot.

Parameters	Initial model	SIMP	BESO	GD
Length of link 1 (m)	0.25			
Length of link 2 (m)	0.19			
Mass of link 1 (kg)	1.0			
Center gravity coordinate of link 1 (m) (in OX; OY; OZ)	0.115; 0; 0			
Inertial moment of link 1 (Kg.m^2) (in OX; OY; OZ) (x10^{-3})	5.81; 5.94; 0.29			
Mass of link 1 2 (kg)	0.448	0.249	0.257	0.279
Center gravity coordinate of link 2 (m) (in OX; OY; OZ)	0.097; 0; 0	0.074; 0; 0	0.076; 0; 0	0.097; 0; 0
Inertial moment of link 2 (Kg.m^2) (in OX; OY; OZ) (x10^{-3})	1.94; 2.03; 0.1	0.067; 0.76; 0.81	0.068; 0.81; 0.87	0.083; 1.49; 1.57

Table PT2. Dynamics analysis results for link 2 pre-TO and after-TO.

Methods	Criteria and evaluation results compared to Pre-TO					
	Mass of link 2	Mass Evaluation	S_{max} (MPa)	Stress Evaluation	D_{max} (mm)	Displacement Evaluation
Pre-TO	0.448	---	0.47	---	5.1 x10^{-4}	Safety
SIMP	0.249	Reduced 44.42%	0.509	Increase 8.3%	9.2 x10^{-4}	Safety
BESO	0.257	Reduced 42.63%	0.58	Increase 23.4%	14.3 x10^{-4}	Safety
GD	0.279	Reduced 37.72%	0.64	Increase 36.17%	7.95x10^{-4}	Safety

According to the analysis results in Table PT2, the SIMP method is well applied to details with 2D geometric structures and motion in a plane. The GD method is not the best choice for this type of structural. In fact, it is not possible to conclude the superiority between the optimal methods for components with complex 3D structures. Moreover, it is clear that the GD method is advantageous when it comes to optimizing structures with many different visual structure options and is not as complicated as when applying the SIMP or BESO methods.

The positions and velocities of the joints are depicted as shown in Fig. P2 and Fig. P3.

The calculation results in Fig. P4 and Fig. P5 show that the driving torque value at the joints has been significantly reduced after optimizing the structure for the link 2. Driving energy cost in the method SIMP is the smallest. However, this result only shows clearly for 2D structures. Even so, this illustrative example clearly demonstrates two important issues including structural optimization is necessary and the difference between the optimization methods is clear. The results of solving the ID problem for the 2DOF robot are described in Fig. P4 and Fig. P5.
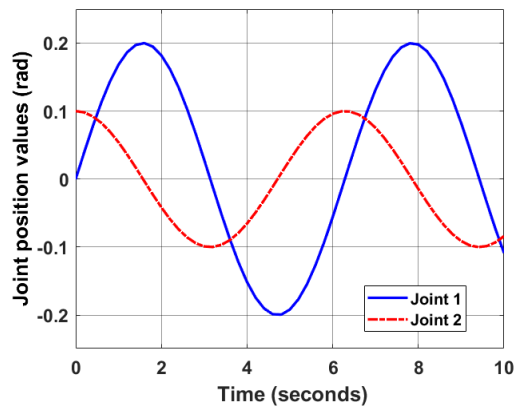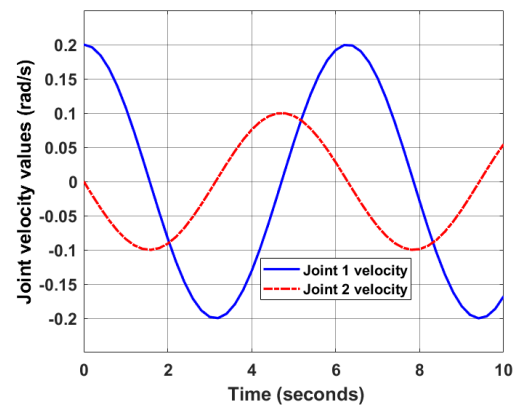

Fig. P2. Joints positions.
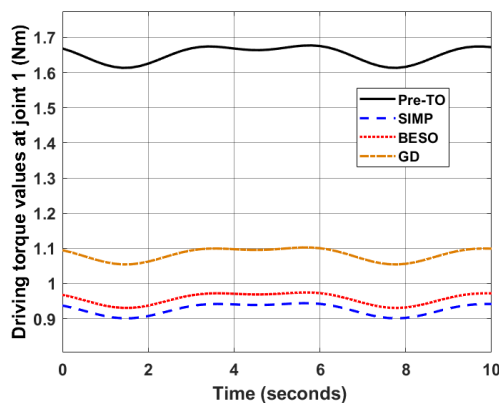

Fig. P3. Joints velocities.
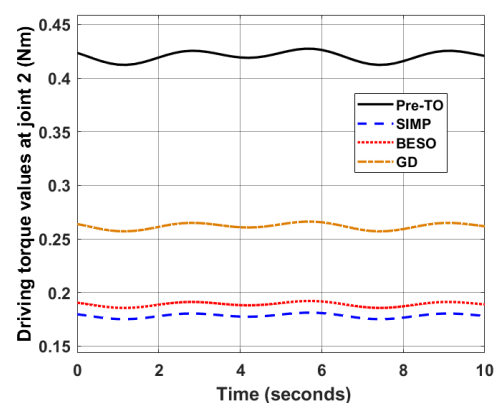

Fig. P4. Torque values at joint 1.

Fig. P5. Torque values at joint 2.

ORCID iD

Duong Xuan Bien⬤ https://orcid.org/0000-0001-7380-8551

Publisher's Note Shahid Chamran University of Ahvaz remains neutral with regard to jurisdictional claims in published maps and institutional affiliations.